RESEARCH ARTICLE

National Science Open
4: 20240025, 2025
https://doi.org/10.1360/nso/20240025

Engineering

Special Topic: Flexible Electronics and Micro/Nanomanufacturing

Body temperature-triggered phase change dry electrode for long-term comfort electroencephalography monitoring

Zekai Wang[#], Haokun Yi[#] & Zhuo Li[*]

Department of Materials Science, Fudan University, Shanghai 200433, China

#Contributed equally to this work.
*Corresponding author (email: zhuo_li@fudan.edu.cn)

Received 2 June 2024; Revised 18 June 2024; Accepted 10 August 2024; Published online 15 August 2024

Abstract: Electrodes are crucial for long-term electroencephalography (EEG) monitoring. Dry electrodes eliminate issues of dehydration, skin irritation, and non-reusability that are associated with wet electrodes. However, overly soft dry electrodes cannot penetrate dense hair, while overly hard electrodes compromise comfort and signal quality. Here, we report a body temperature-triggered, phase change dry electrode to address these problems. The electrode, made from a polymer composite with crystalline region and silver flakes, is rigid at room temperature, allowing it to pass through hair. Upon contact with the scalp, body temperature melts the crystalline region, significantly reducing the modulus, thereby enhancing comfort and reducing contact impedance. This phase transition also transforms the electrode into a pressure sensitive adhesive, ensuring the stable contact. Additionally, its shape memory effect enables the electrode to return to its original shape, making it reusable. The reported electrodes exhibit superior signal quality and stability in long-term EEG monitoring.

Keywords: phase change, crystalline melting transition, electroencephalography monitoring, conductive composite, dry electrode

INTRODUCTION

Long-term monitoring of electroencephalography (EEG) signals is crucial for various applications, including disease diagnosis [1], emotion recognition [2], and brain-computer interface (BCIs) [3]. However, EEG signal collection is challenging due to the inherently weak signals and the obstacle posed by dense hair. As essential components facilitating electrical communication between the body and external devices [4], electrodes must meet several criteria for effective long-term EEG monitoring: they must penetrate dense hair to establish stable scalp contact, maintain low contact impedance for high signal quality, and ensure comfort for long-term monitoring.

Traditional wet electrodes, such as Ag/AgCl electrodes or gold cup electrodes with conductive paste/gel, are the clinical gold standard due to their intimate scalp contact and low impedance. However, the use of conductive paste or gel increases the risk of short circuits between adjacent electrodes, is difficult to clean due to the adherence to hair, and degrades signals as it dries over time [5]. Semi-dry electrodes with large liquid reservoirs in the form of sponge [6] or aerogel [7] address dehydration issues but retain other drawbacks of wet electrodes. Dry electrodes, featuring claw [8] or comb [9] shapes, obviate the need for

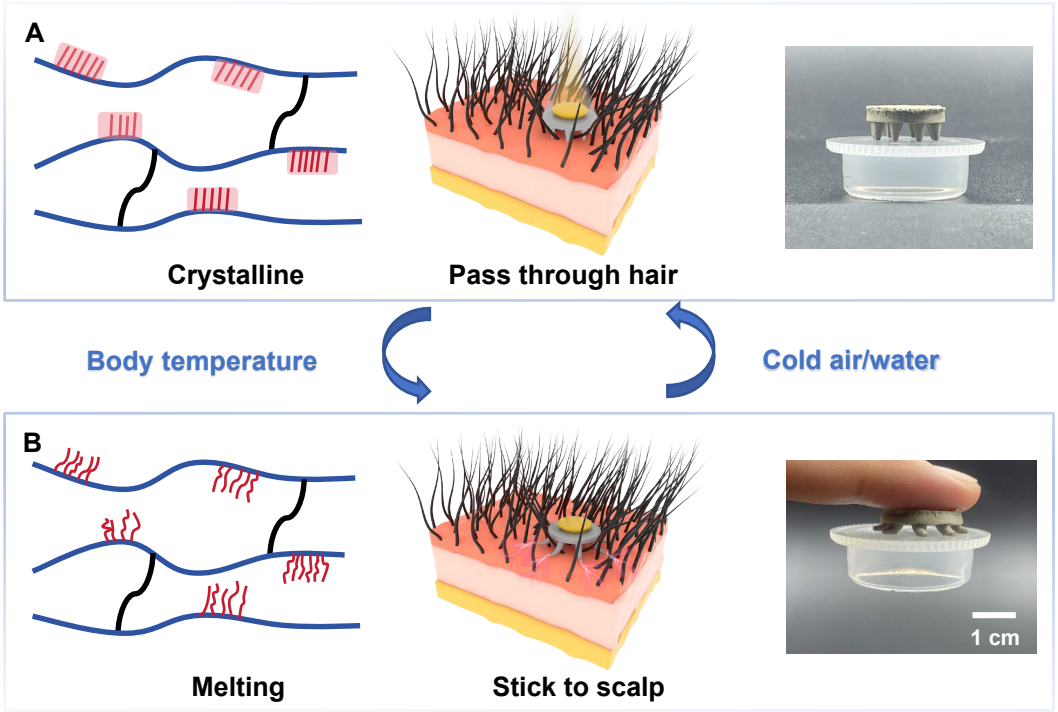

Figure 1 Schematical illustration of the PCE. (A) At room temperature, the crystalline structure renders a high modulus, which allows the PCE to effectively penetrate hair to contact with the scalp. (B) Upon contact with the scalp, the body temperature causes the crystalline part to melt, softening the PCE, increasing the contact area, and making it self-adhesive to the scalp.

conductive paste/gel and are favored for long-term monitoring. Traditional metal dry electrodes, with sufficient stiffness, can easily comb through hair and make direct contact with the scalp. However, rigid metal electrodes are uncomfortable for long-term wear, and their non-conformal contact with the scalp leads to high impedance and poor signal quality [10]. In contrast, soft dry electrodes, such as those made of conductive elastomer composites [11], offer enhanced comfort and may even be engineered to adhere to the scalp, improving the contact between the electrode and scalp [12]. However, these soft electrodes deform under dense hair and impede scalp contact, making them more suited to non-hair or short-hair regions. Given the limitations of these single-phase electrodes, recent research has focused on developing electrodes with phase transition properties. Most reported work involving liquid-solid transitions [13,14], where the initial liquid state facilitates permeation through hair and subsequent solidification, based on curing [13] or sol-gel transitions [14], establishes stable scalp contact. Yet, these electrodes still pose challenges in post-test cleaning and are not reusable, leading to higher costs and material waste.

In this report, we aim to address these issues by using a dry electrode based on a conductive composite featuring a rigid-soft phase transition, instead of employing a liquid-solid phase transition. This composite, referred to as a phase change composite (PCC), comprises a polyacrylate matrix containing crystallizable long alkyl side chains and silver flakes as conductive fillers. By adjusting the cross-linking density of the polymer matrix, it exhibits a melting temperature (T_m = 33.2°C) close to body temperature. For the prepared phase change electrode (PCE), at room temperature (25°C), the crystalline structure imparts a high Young's modulus of 15.0 MPa, enabling the electrode to effectively pass through hair (Figure 1A). Upon contact with the scalp, body temperature triggers the melting of the crystalline region, resulting in a dramatic drop in modulus

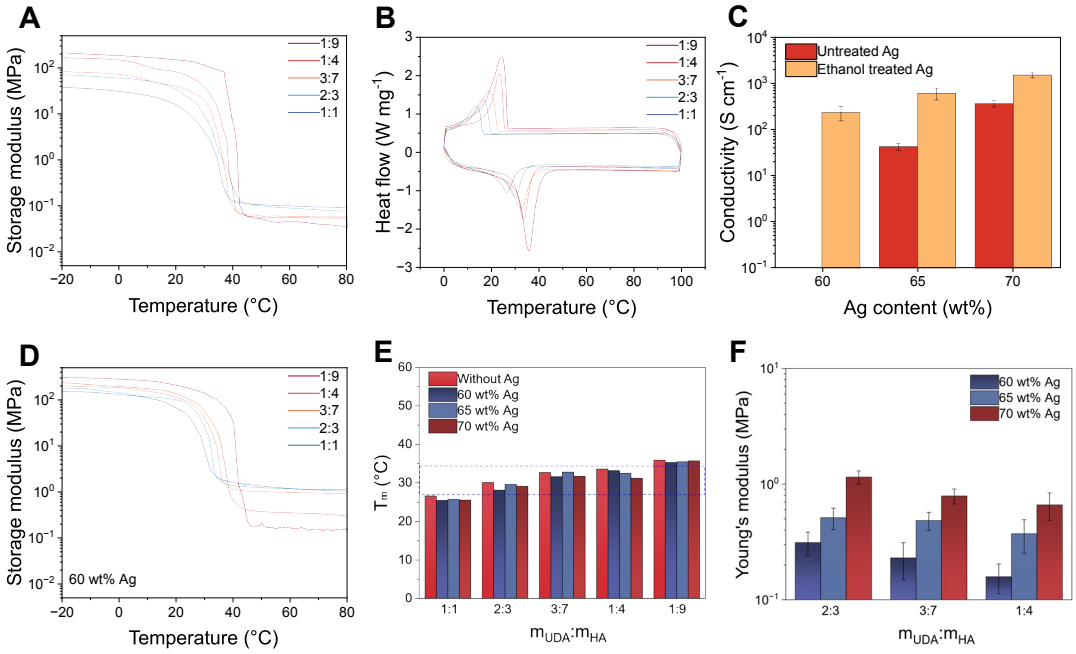

Figure 2 (A) DMA curves of UDA-HA polymers with different UDA and HA mass fractions. (B) DSC curves of UDA-HA polymers with different UDA and HA mass fractions. (C) Electrical conductivity of PCCs (m_{UDA}:m_{HA} = 1:4) with untreated silver flakes and boiling ethanol-treated silver flakes respectively. (D) DMA curves of PCCs with 60 wt% Ag. (E) Comparison of T_m of UDA-HA polymer matrices and PCCs. (F) Young's modulus of different PCCs at 36.5°C.

to 0.158 MPa. This softened electrode improves contact with the scalp, thereby reducing contact impedance and enhancing comfort (Figure 1B). Additionally, the substantial increase in adhesive dissipation energy allows the softened electrode to adhere to the skin, further enhancing the stability in long-term monitoring. Moreover, when cooled with cold air or water, the PCE hardens and loses its adhesive properties, facilitating its removal from the scalp. Upon reheating above its T_m, the PCE recovers its original shape due to the shape memory effect, ensuring its reusability. The PCE demonstrated superior performance in monitoring high-quality EEG signals compared to commercial wet electrodes, both during long-term monitoring and repeated use.

RESULTS

Materials design for PCEs

The polyacrylate matrix is synthesized through a free radical reaction between hexadecyl acrylate (HA) and urethane diacrylate (UDA), the structures of which are illustrated in Figure S2A. HA, characterized by its long alkyl chain, exhibits a crystalline-melting transition with a crystallization temperature (T_c) of 13.6°C and a T_m of 18.8°C, according to its differential scanning calorimetry (DSC) curve (Figure S2B). UDA, a bifunctional aliphatic polyurethane acrylate, serves as a large-molecule cross-linking agent. By varying the ratio of UDA to HA, the cross-linking density can be adjusted, producing a series of polymers with T_m values ranging from 22.6 to 35.6°C. These polymers, denoted as UDA-HA, all exhibit clear phase change behaviors, as shown in the dynamic mechanical analysis (DMA) curves (Figure 2A). With increasing HA content, T_m rises because higher temperatures are required to melt more crystalline long alkyl side chains. In addition,

above T_m, higher HA content results in more crystalline regions, leading to a higher storage modulus in the rigid state; below T_m, higher HA content implies a lower cross-linking density, resulting in a lower storage modulus (G') in the soft state [15]. In other words, increasing the HA content leads to a greater change in modulus during the phase transition. The DSC results (Figure 2B) exhibit a similar trend in T_m variation to that observed in DMA (ranging from 26.3 to 35.8°C, Figure S3). As HA content increases, both T_m and melting enthalpy values increase in the DSC curves.

To ensure effective transmission of electrophysiological signals, electrodes need to be highly conductive. Silver flakes, a commonly used filler for conductive composites, were incorporated into the UDA-HA matrix for this purpose. Considering that maintaining a low modulus in the soft state is crucial for both wearing comfort and minimizing contact impedance, achieving equivalent conductivity with a lower fraction of silver micro-flakes is preferred. The conductivity of the composite is heavily dependent on the surface conditions of the silver flakes. Insulating surface lubricants, typically long-chain fatty acids from the manufacturing process, significantly hinder the composites' conductivity [16]. Our previous study found that boiling ethanol treatment effectively removes these fatty acids and chemically reduces the coordinated silver carboxylate to silver nanoparticles [17], thus enhancing the conductivity of PCCs. Therefore, we treated the silver flakes with boiling ethanol to improve conductivity and reduce filler content. As shown in Figure S4, the surface morphology of the silver flakes becomes rougher after ethanol treatment, with small silver particles adsorbed on the flakes. This indicates the removal of some lubricants from the silver surface and the generation of nanoparticles. Thermogravimetric analysis (TGA) tests were used to quantify the amount of surface lubricant, as these organic compounds decompose at elevated temperatures while pure silver remains. As shown in Figure S5, the residual mass at 600°C increased from 98.87% to 99.47% after ethanol treatment, indicating a decrease in the amount of lubricants. X-ray photoelectron spectroscopy (XPS) high-resolution spectra confirmed this by showing a significant reduction in the C=O peak from carboxyl groups after ethanol treatment (Figure S6). These analyses suggest that most insulating lubricants were removed, exposing highly conductive silver and thereby enhancing conductivity. The electrical conductivity of PCC (m_{UDA}:m_{HA} = 1:4) was compared when incorporating untreated silver flakes versus ethanol-treated silver flakes (Figure 2C). Without surface treatment, the PCC with 60 wt% silver flakes is not conductive, while the conductivities are 43.3 and 366.2 S/cm at 65 wt% and 70 wt%, respectively. In contrast, after boiling ethanol treatment, the electrical conductivity of PCC is already 236.0 S/cm at 60 wt% and reaches 1516.7 S/cm at 70 wt%. Additionally, the different UDA-HA matrices have minimal influence on electrical conductivity (Figure S7), indicating that conductivity primarily depends on the surface state of the silver. Therefore, in our subsequent composites, we exclusively use ethanol-treated silver flakes.

For electrode preparation, the most suitable PCC must meet several criteria. First, the transition temperature T_m should be slightly below body temperature (approximately 36.5°C) to enable a body temperature-driven crystalline-melting transition. However, the T_m should not be too low to prevent premature softening, which would make it difficult for the electrode to pass through the hair. Additionally, the material should have a low Young's modulus in the soft state and low skin-electrode contact impedance to enhance wearing comfort and signal quality during long-term EEG monitoring.

We first screened PCCs based on their T_m. As shown in the DMA curves (Figure 2D) and DSC curves (Figure S8), the introduction of silver did not notably impact their T_m, with the variation within 2.5°C. We selected PCCs with T_m between 27.0 and 34.5°C (above room temperature and below body temperature, as

shown in the blue dashed box in Figure 2E) and excluded PCCs with UDA:HA ratios of 1:9 and 1:1. Subsequently, the moduli of the remaining nine samples in the soft state at 36.5°C were compared. From the DMA test results (Figure 2D), it was found that the incorporation of silver increases the G' both in the soft and rigid states, while maintaining a modulus change approaching two orders of magnitude over the transition. In addition, similar to the pure polymer matrices, a higher HA content results in a lower Young's modulus. The tensile tests also show that fewer silver flakes and higher HA content lead to reduced Young's modulus in the soft state (Figure 2F, representative stress-strain curves are shown in Figure S9). Consequently, $PCC_{1\text{-}4\text{-}60}$ with the highest HA content and lowest silver loading has the lowest modulus among the nine samples. Moreover, the trend of skin-electrode contact impedance aligns with that of Young's modulus. $PCC_{1\text{-}4\text{-}60}$ not only exhibits lower contact impedance compared to other PCCs with the same silver content (Figure S10A), but also demonstrates lower impedance than PCC (m_{UDA}:m_{HA} = 1:4) with increased silver content despite the latter's higher conductivity (Figure S10B). Based on these experimental results, we have selected $PCC_{1\text{-}4\text{-}60}$ as the electrode material, referred to as PCE, for subsequent tests.

Properties of PCEs

The body temperature-triggered change in mechanical properties of PCE is demonstrated by the tensile test, as shown in Figure 3A. At 25.0°C, Young's modulus of PCE is 15.0 MPa and can be stretched to 76.7%. This rigidity at room temperature enables the claw-shaped electrode to effectively penetrate the hairy region and reach the scalp (Figure S11). After reaching 36.5°C, Young's modulus exhibited a notable reduction to 0.158 MPa while the stretchability increased to 310.1%. The soft and stretchable conductive composite is beneficial for the conformal coverage on the contact surface (Figure 3B).

Moreover, the significant change in modulus leads to noticeable variations in the adhesive properties of PCE, resulting in a temperature-controlled reversible adhesion effect. As shown in Figure 3C, at 36.5°C, PCE demonstrates a peeling strength of 29.6 N/m on pig skin. In contrast, at 25.0°C, the peeling strength of PCE is only 2.2 N/m. In its soft state, PCE adheres firmly to the skin, and its adhesion capability can lift various objects such as metallic spoons, plastic centrifuge tubes, glass bottles, and ceramic pestles (Figure 3D). This adhesion behavior is attributed to the soft viscoelastic properties of PCE, which makes it a pressure-sensitive adhesive (PSA) at 36.5°C. For PSAs, adhesion occurs during a low-frequency process when the adhesive flows and wets the substrate under gentle pressure, while debonding involves high-speed deformation of the adhesive layer under stress [18]. The viscoelastic window is a well-established method for predicting PSA performance based on its viscoelastic properties [19]. At 25.0°C, the G' of PCE far exceeds the Dahlquist criterion (the maximum value allowed to function as a PSA, usually 0.3 MPa,) [20], indicating its lack of capability to become a PSA. At 36.5°C, PCE well resides within the high shear PSA region (Figure S12), providing sufficient adhesion strength for various surfaces, debonding on demand, and maintaining consistent adhesion strength through multiple bond-debond cycles (e.g., 20 cycles as shown in Figure S13).

Upon contact with the scalp, PCE is heated by the skin and becomes soft. The thermal transport from the skin to PCE was investigated to verify that this transition can be driven by body temperature. We simulated the transport process, based on the thermal conductivity and specific heat of PCE at 25.0°C (Table S1). The result shows that the top of the claw can reach 33.2°C (T_m of PCE) within 545 s (Figure 3E), which is sufficient to trigger the phase transition of PCE, and after 1800 s, the heat transfer stabilizes.

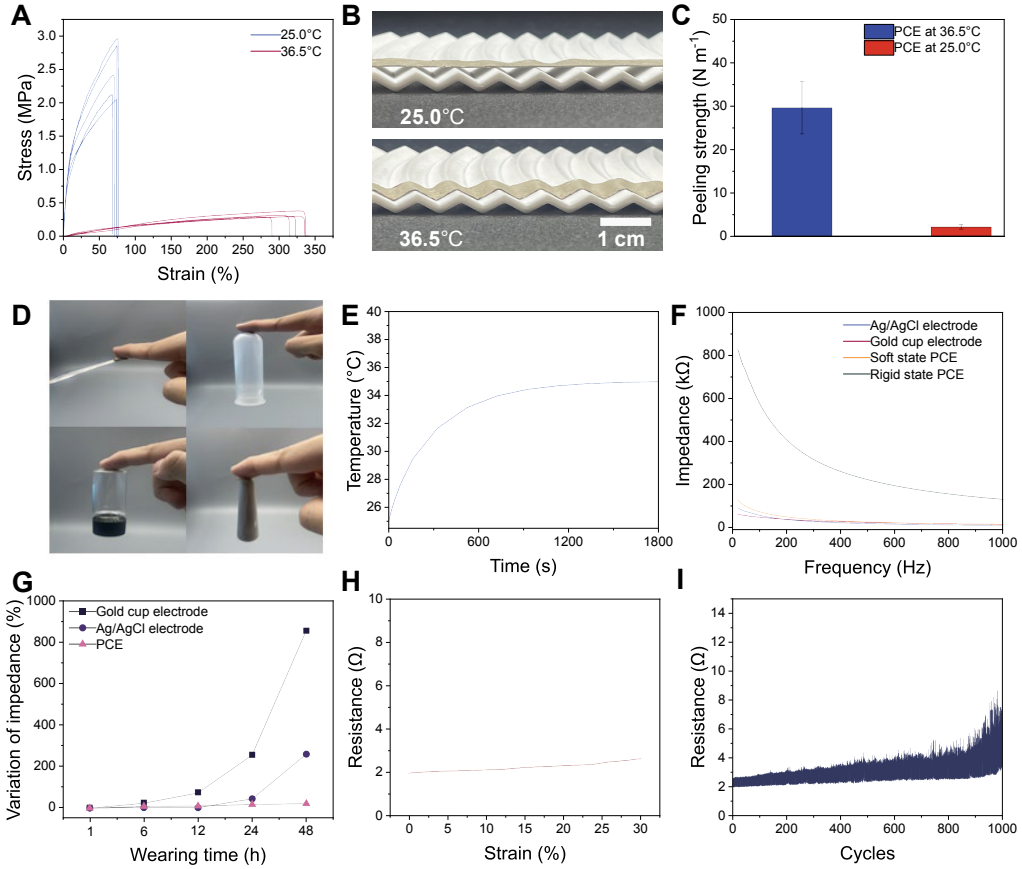

Figure 3 (A) Stress-strain curves of PCE at 25.0 and 36.5°C. (B) The body-temperature-driven reduction in modulus of PCE allows it to conformally contact with the wavy substrate. (C) The 90° peeling strength of PCE at 25.0 and 36.5°C respectively. (D) PCE can be adhered to different objects, such as the metallic spoon (about 5 g), plastic centrifuge tube (about 15 g), glass bottle (about 20 g), and ceramic pestle (about 25 g). (E) Heat transfer curve at the top of the claw of the PCE. (F) Skin-electrode contact impedance of the Ag/AgCl electrode, gold cup electrode, rigid state PCE and soft state PCE. (G) Variation of contact impedances of different electrodes after 48 h of wearing (@ 100 Hz). (H) Resistance of PCE when stretched 30% at 36.5°C. (I) Resistance of PCE when stretched for 1000 cycles at 36.5°C under 30% strain.

To demonstrate the effectiveness of PCE in reducing impedance after softening, impedance tests were conducted on PCE before and after softening, and compared with commercial wet electrodes (Figure 3F). The impedance at 100 Hz for PCE is reduced significantly from 589.0 to 75.4 kΩ after phase transition, which is slightly higher than the Ag/AgCl electrode and gold cup electrode (75.4 vs. 49.3 and 58.9 kΩ, respectively). We also recorded impedance change over two days' wearing. As shown in Figure 3G, within the first 6 h, there were no significant impedance changes for any of the electrodes at 100 Hz. However, after 12 h, the impedance of the gold cup electrode increased, and continued to increase afterwards. The Ag/AgCl electrode showed relatively small impedance changes within 24 h due to the protective tape, but there was a significant increase (2.57 times compared to 1 h) after 48 h due to the gradual drying of the gel. In contrast, the impedance of the PCE remained relatively stable after 48 h of wearing, highlighting the advantages of PCE for long-term monitoring.

PCE in its soft state also exhibits high stability under cyclic deformation and sweating, which is beneficial for long-term monitoring. We recorded the variation in resistance of PCE when stretched by 30% at 36.5°C, as 30% is the inelastic deformation limit of human skin [21]. At this strain, the resistance only changed by

30.7% which even included the change resulting from dimensional variations (Figure 3H). As evidenced by the scanning electron microscopy (SEM) image (Figure S14), the silver flakes are aligned parallel within the UDA-HA matrix, which ensures consistent contact between the flakes during stretching and thus minimizing resistance fluctuations. We also performed 1000 cycles of 30% tensile tests (Figure 3I and Figure S15), PCE showed a low hysteresis and high cyclic stability, only producing a permanent deformation of about 3.6% after 1000 cycles. The resistance changed by 10% within the first 200 cycles. Subsequently, the resistance fluctuation increased, yet the maximum resistance remained within 8.6 Ω at 30% strain, ensuring the PCE's electrical communication capability under cyclic deformations. Sweating is a common issue during long-term wearing, so we tested PCE's stability against immersion in simulated sweat for 28 d. As shown in Figure S16, after 7 d of continuous immersion, the resistance of PCE remained unaltered, and after 28 d of immersion, the resistance only changed by 18.75%. Additionally, the PCE maintained its integrity without any delamination (as shown in the inset of Figure S16).

Because the electrode is in direct contact with the skin, the biocompatibility and wearing comfort of the PCE were evaluated. Figure S17A shows a tissue section of Sprague-Dawley (SD) rat skin after 72 h of electrode attachment, compared to a nearby tissue section without the electrode (Figure S17B). No inflammatory reaction was observed with PCE attachment. Additionally, to assess wearing comfort, we pressed two electrodes: PCE and an electrode made from Ag/polydimethylsiloxane (PDMS) composite (with Young's modulus of approximately 3 MPa), onto the skin and fixed them with an elastic bandage. After wearing for 12 h, both electrodes were removed. As shown in Figure S18, upon removal, the trace left by the Ag/PDMS electrode was deeper compared to that of the PCE, and the trace area of the PCE was larger relative to the Ag/PDMS, attributed to the lower modulus of PCE at body temperature. After 20 min, the trace of the PCE had mostly disappeared, while remnants of the Ag/PDMS trace remained, indicating better wearing comfort of PCE compared with the traditionally accepted soft PDMS composite electrode [22].

Moreover, due to its phase change and cross-linking structure, PCE exhibits shape memory performance (Movie S1), which is beneficial for multiple uses. DMA tests (Figure S19) quantified the shape memory performance of PCE. Under strains greater than 50%, the shape recovery rate of PCE can reach 97.1%. After the use of the electrode, applying cold water or blowing cold air makes it hard and non-sticky again, facilitating easy removal from the scalp. Immersing the electrode in an environment above the transition temperature helps it recover its original shape, making it ready for the next use (Movie S2). The repeated use of PCE for recording EEG will be presented in the next section.

Application

EEG signals originate from the simultaneous electrical discharges of many pyramidal cells in the brain, generating electric fields that are detectable on the scalp. Based on their frequency, EEG signals can be classified into δ waves (0.2–3.5 Hz), θ waves (4–7.5 Hz), α waves (8–13 Hz), β waves (14–30 Hz), and γ waves (30–90 Hz) [23]. Among them, α waves, associated with relaxation in the brain, show significant enhancement around 10 Hz when the subjects relax and close their eyes, making this a commonly used EEG test [24]. We detected α waves using both PCE and gold cup electrodes as a benchmark. As shown in Figure S20, the α rhythm was suppressed for both PCE and the wet electrode during the eyes-open condition, while a distinct α rhythm around 10 Hz was observed during the eyes-closed condition. To demonstrate the PCE's

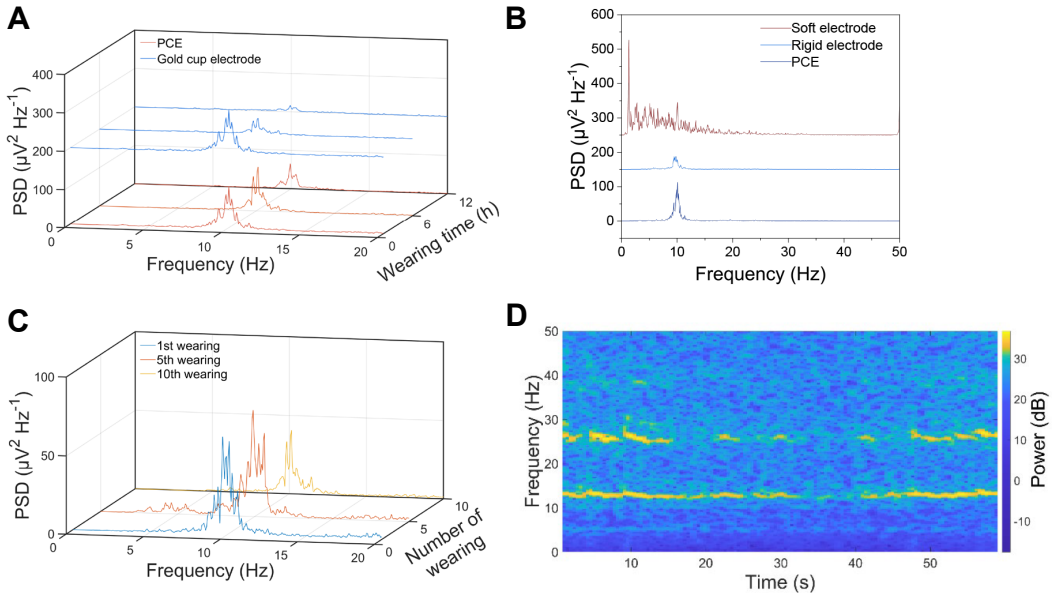

Figure 4 (A) PSD plots for wearing durations of 1, 6, and 12 h during the eyes-closed condition. (B) EEG signals acquired by PCE as compared to simplex soft and hard electrodes during the eyes-closed condition. (C) EEG signals acquired by the PCE under repeated wearing during the eyes-closed condition. (D) Time-frequency plot of SSVEP signal acquired by PCE at 13 Hz stimulation frequency.

ability to monitor EEG signals as effectively as the wet electrode, the correlation coefficient between the time-domain signals acquired by both electrodes was calculated. The results showed a high degree of correlation, with correlation coefficients of 0.88 for the eyes-open condition and 0.95 for the eyes-closed condition.

In order to demonstrate the advantage of PCE in long-term EEG monitoring, a volunteer wore both types of electrodes for 12 h, and the EEG signals during the eyes-closed condition were recorded (Figure 4A). Due to the drying of conductive paste, the impedance of the gold cup electrode increased, leading to a gradual decrease in the power of α wave signals. In contrast, the PCE consistently maintained a high level of power even after 12 h wearing.

To further illustrate the necessity of a phase transition during EEG monitoring, we compared the performance of PCE with a simplex soft electrode (Ecoflex/Ag, 70 wt% Ag, modulus around 500 kPa) and a hard electrode (rigid-state PCE before phase transition) in acquiring α wave signals (Figure 4B). The signals acquired by the Ecoflex/Ag electrode exhibited significant low-frequency noise due to its inability to penetrate through dense hair. The trapped hairs between the electrode and the scalp increased the noise ratio. In contrast, clear α wave signals were effectively acquired by PCE. However, without undergoing a phase transition, the signals acquired by rigid-state PCE were relatively weak because of the limited contact with the scalp and high contact impedance (Figure 3F). Only the PCE that underwent a phase transition could effectively penetrate the hair and exhibit strong and clear α wave signals.

Additionally, because PCE does not involve a liquid phase and possesses a shape memory effect, it can be reused. We conducted α wave tests on the same subject with the same electrode worn repeatedly. EEG signals were recorded during the 1st, 5th, and 10th wearings. The power spectral density (PSD) plots (Figure 4C) consistently exhibited significant enhancement at 10 Hz across all trials, indicating that the PCE can be effectively reused for EEG testing.

To explore the feasibility of PCE in other applications, we also tested the steady-state visually evoked

potential (SSVEP) signal, another common EEG signal. During the testing process, volunteers observe visual stimuli presented at a certain frequency or with continuously changing frequencies. Neural networks corresponding to the stimulation frequency or its harmonic frequencies resonate, causing continuous responses in the brain's visual cortex region and forming the SSVEP signal [25]. By analyzing the frequency peaks in the frequency domain plot, it is possible to determine the stimulus on which the subject is focused. Therefore, SSVEP can be used to identify the intentions of subjects, which is common in BCI applications [3]. In the SSVEP test, electrodes were placed in the same positions as described in the previous tests. The flicker frequency of the light-emitting diode (LED) was adjusted to 13 Hz, and the volunteer sat quietly observing the flicker from a distance of 0.6 m. The obtained SSVEP signal, as shown in Figure 4D, exhibits a clear enhancement at 13 Hz as well as a noticeable response at the harmonic frequency of 26 Hz, consistent with the characteristics of SSVEP signals, demonstrating PCE's promising application in the field of BCI.

CONCLUSIONS

In summary, we report a body temperature-triggered phase change in dry electrodes for EEG monitoring. The electrode incorporates a crystalline region within the polymer matrix and utilizes boiling ethanol-treated silver flakes as the conductive fillers. At room temperature, the electrode remains in the crystalline state, providing the rigidity necessary to pass through hair and make direct contact with the scalp. Upon reaching the scalp, the body temperature-driven melting of the crystalline part results in two orders of magnitude decrease in modulus, transforming it into a PSA. The enhanced softness and adhesiveness increase the contact area, reduce impedance, and ensure wearing comfort for long-term monitoring. In addition, the shape memory effect of the dry electrode allows for reusability, making it suitable for multiple uses. These advantages were demonstrated in a long-term (12 h) monitoring session as well as during repeated wearing sessions. The collected EEG signals exhibited similar results to those obtained from wet electrodes, with no signal degradation with time, indicating its promise for medical diagnosis and BCI applications.

METHODS

Materials

UDA (CN9021NS) was purchased from Sartomer. HA (guaranteed reagent, > 90%) was purchased from Aladdin. Benzoyl peroxide (BPO, AR) was purchased from Macklin. Silver flakes (AgF-3C, average size: 2.3 μm) were purchased from Ningxia New Materials Corporation. Ethanol (AR) was purchased from Sinopharm Chemical Reagent Co., Ltd. Tissue fixative (4%) was purchased from Servicebio. Simulated sweat (pH 4.7) was purchased from Dongguan Xinheng Technology Co., Ltd. Conductive paste (Ten 20) was purchased from Weaver and Company. All materials were used as received.

Preparation of UDA-HA

A certain amount of UDA was weighed in a beaker and then placed in a 50°C water bath to decrease its

viscosity. Then a certain amount of HA was added to the beaker (m_{UDA}:m_{HA} = 1:1–1:9) along with 0.3 wt% of the thermal initiator BPO. The above solution was stirred at 100 r/min for 2 h to ensure complete mixing. Finally, the mixture was poured into polytetrafluoroethylene (PTFE) mold, and the air bubbles in the precursor solution were removed by vacuum. Once the air bubbles were completely removed, the solution was heated and cured under pressure at 80°C for 2 h.

Surface treatment of the silver flakes

Silver flakes (5 g) and ethanol (200 mL) were added to a beaker and were heated and stirred (80°C, 500 r/min) for 10 min. The supernatant was removed after the precipitation of silver. This process was repeated three times. The silver flakes were then collected by filtration and placed in a vacuum oven to dry for 24 h. Finally, a 200-mesh sieve was used to obtain silver flakes with a more uniform size.

Preparation of PCC and PCE

The above ethanol-treated silver flakes (60 wt%–70 wt%), UDA-HA mixture (m_{UDA}:m_{HA} = 1:1–1:9 and 0.3 wt% BPO) was added into the mortar and fully ground and mixed for 20 min. The mixture was poured into the PTFE mold and the air bubbles were removed by vacuum before curing at 80°C for 2 h and 160°C for 1 h under pressure.

The PCE is designed in a claw-shaped form (8 claws with an electrode diameter of 16.0 mm, a total electrode height of 6.3 mm, an upper diameter of the claw of 2.4 mm, a lower diameter of the claw of 0.9 mm, and a height of the claw of 3.8 mm). The wiring of the electrode to the test equipment can be made by burying the copper wire into the prepolymer solution of the electrode material and curing it together with the electrode material.

Characterization of UDA-HA, silver flakes, PCC and PCE

The dynamic mechanical analyzer (DMA Q800, TA Instruments, USA) was used to test the dynamic mechanical properties of UDA-HA and PCC. To measure the phase transition, the sample was heated from −20°C–80°C with a ramping rate of 3°C/min at 0.1% strain. To measure the viscoelastic properties at different frequencies, a frequency sweep from 0.1 to 20 Hz at 36.5°C was performed. Dog bone shaped samples were used in DMA tests of 10.0 mm length, 2.0 mm width and 1.0 mm thickness with tension mode. The differential scanning calorimeter (DSC Q200, TA Instruments, USA) was used to test the T_c and T_m of UDA-HA and PCC. The conditions for the DSC test were: 0–100°C, a heating rate of 10°C/min and a cooling rate of 10°C/min. TGA was conducted on a thermal gravitational analysis apparatus (TG 209 F1 Libra, Netzsch, Germany) at a heating rate of 10°C/min from 30 to 600°C. The morphologies of silver flakes and PCC were captured by scanning electron microscope (Sigma 300, ZEISS, Germany) at an acceleration voltage of 3.0 kV. XPS spectrum was conducted on an XPS spectrometer (Thermo Scientific K-Alpha+, ThermoFisher, USA) with 1486.6 eV monochromatic AlKα source (Mono AlKα) at 15.0 kV, 15.0 mA beam current and CAE analyzer scanning mode. Conductivity was measured by a four-probe metal/semiconductor resistivity meter (SB100A-2, Shanghai Qianfeng Electronic Instrument, China). Five parallel specimens were used in each sample.

Mechanical tests were conducted on the electronic universal material testing machine (CMT-4304-QY, Shenzhen Sans Instruments, China) at a speed of 5 mm/min. Dog bone shaped samples were used in mechanical tests of 16.0 mm length, 2.0 mm width and 1.0 mm thickness. Five parallel specimens were used in each sample. Resistance was measured by source measure unit (2450 SourceMeter, Keithley, USA). Skin-electrode contact impedance was measured by a precision inductance, capacitance, resistance (LCR) meter (E4980AL, Keysight, USA) from 20 to 1000 Hz. Before the test, the skin was wiped with 75% alcohol swabs. A 90-degree peeling test was conducted on the electronic universal material testing machine (CMT-4304-QY, Shenzhen Sans Instruments, China) at a speed of 100 mm/min, The sample with a dimension of 100.0 mm length, 10.0 mm width and 200 μm thickness was attached to the pig skin. In order to prevent deformation of the sample during the peeling process, a 100.0 mm × 10.0 mm × 100 μm polyimide (PI) tape was applied to the top layer of the sample as a backing layer. The debonding frequency was calculated by dividing the peeling speed by the thickness of the peeling sample. The DMA (Q800, TA Instruments, USA) was also used to evaluate the shape memory performance of the PCE under "controlled force" mode, with a temperature ramp from 0 to 70°C at a heating rate of 10°C/min and a subsequent cooling rate of 5°C/min. Thermal conductivity and specific heat were measured using a laser flash apparatus (LFA467, Netzsch, Germany). Thermal simulation was conducted on COMSOL Multiphysics® 6.1. In order to evaluate the biocompatibility of the electrode, the electrode was attached to the back skin of the SD rat. After 72 h of normal rearing, the rat skin at the electrode site was removed and fixed with 15 mL of tissue fixative. Subsequently, the fixed skin was embedded in paraffin, sectioned longitudinally, dehydrated and sealed, and stained using hematoxylin-eosin staining (HE staining). Finally, the stained tissue sections were observed using a digital section scanner (Pannoramic MIDI II, 3DHISTECH, China). The animal experiment was approved by the Animal Care and Use Committee of Fudan University (Approval Number: 202109014S).

EEG test

The EEG signals were measured using an Openbci Cyton Biosensing Board (8-channels, Openbci, USA) with a sampling rate of 250 Hz. Three electrodes were placed in A1, A2, and O1 zones according to the international 10–20 EEG system, a standard system for electrode positioning, as shown in Figure S1. The electrodes were fixed with an elastic bandage. The acquired signals were filtered by MATLAB R2023a (including 48–52 Hz notch filtering and 0.5–50 Hz bandpass filtering). PSD plots were also acquired through MATLAB R2023a. In order to compare the correlation between the EEG signals acquired by the PCE and the gold cup electrode (the gold cup electrode mentioned was used with conductive paste), the gold cup electrode was placed next to the PCE on the O1 zone side to acquire the signals simultaneously, and the correlation coefficient of the signals acquired by the two electrodes was calculated using Eq. (1) [26]:

$$\rho_{X,Y} = \frac{\mathrm{cov}(X,Y)}{\sigma_X \sigma_Y} = \frac{\sum_{i=1}^{N}\left(X_i - \overline{X}\right)\left(Y_i - \overline{Y}\right)}{\sqrt{\sum_{i=1}^{N}(X_i - \overline{X})^2}\sqrt{\sum_{i=1}^{N}(Y_i - \overline{Y})^2}}, \quad (1)$$

where ρ represents the correlation coefficient, cov represents the covariance of the two sets of signals, σ represents the standard deviation, X and Y, denoted as X_i and Y_i ($i = 1, 2, 3, \ldots, n$), are EEG data series from the PCE and gold cup electrode, and $\overline{X}$ and $\overline{Y}$ are the sample means of X and Y respectively. The closer the value of ρ is to 1, the more correlated the two sets of signals are.

Data availability

The original data are available from corresponding authors upon reasonable request.

Acknowledgements

We are grateful for the useful discussion with Prof. Yajie Qin, Mr. Yizhou Jiang and Mr. Weiming Hu from the School of Information Science and Technology, Fudan University.

Funding

This work was supported by the National Natural Science Foundation of China (U22A20249, 52173071).

Author contributions

Z.L., H.Y. and Z.W. designed the experiment. Z.W. conducted the experiments and analyzed the data. Z.W. wrote and edited the manuscript under the supervision of Z.L.

Conflict of interest

The authors declare no conflict of interest.

Supplementary information

The supporting information is available online at https://doi.org/10.1360/nso/20240025. The supporting materials are published as submitted, without typesetting or editing. The responsibility for scientific accuracy and content remains entirely with the authors.

References

1 Mumtaz W, Xia L, Ali SSA, *et al.* Electroencephalogram (EEG)-based computer-aided technique to diagnose major depressive disorder (MDD). *BioMed Signal Process Control* 2017; **31**: 108–115.

2 Zheng WL, Zhu JY, Lu BL. Identifying stable patterns over time for emotion recognition from EEG. *IEEE Trans Affect Comput* 2019; **10**: 417–429.

3 Spüler M, Zhang D. A high-speed brain-computer interface (BCI) using dry EEG electrodes. *PLoS ONE* 2017; **12**: e0172400.

4 Yuk H, Lu B, Zhao X. Hydrogel bioelectronics. *Chem Soc Rev* 2019; **48**: 1642–1667.

5 Li GL, Wu JT, Xia YH, *et al.* Review of semi-dry electrodes for EEG recording. *J Neural Eng* 2020; **17**: 051004.

6 Lin S, Liu J, Li W, *et al.* A flexible, robust, and gel-free electroencephalogram electrode for noninvasive brain-computer interfaces. *Nano Lett* 2019; **19**: 6853–6861.

7 Wang J, Zhou Q, Wang A, *et al.* Sponge inspired flexible, antibacterial aerogel electrode with long-term high-quality electrophysiological signal recording for human-machine interface. *Adv Funct Mater* 2024; **34**: 2309704.

8 Xing X, Wang Y, Pei W, *et al.* A high-speed SSVEP-based BCI using dry EEG electrodes. *Sci Rep* 2018; **8**: 14708.

9 Huang YJ, Wu CY, Wong AMK, *et al.* Novel active comb-shaped dry electrode for EEG measurement in hairy site. *IEEE Trans Biomed Eng* 2015; **62**: 256–263.

10 Salvo P, Raedt R, Carrette E, *et al.* A 3D printed dry electrode for ECG/EEG recording. *Sens Actuat A-Phys* 2012; **174**: 96–102.

11 Lin CT, Liao LD, Liu YH, *et al.* Novel dry polymer foam electrodes for long-term EEG measurement. *IEEE Trans Biomed Eng* 2011; **58**: 1200–1207.

12 Zhang L, Kumar KS, He H, *et al.* Fully organic compliant dry electrodes self-adhesive to skin for long-term motion-robust epidermal biopotential monitoring. *Nat Commun* 2020; **11**: 4683.

13 Luo J, Sun C, Chang B, *et al.* MXene-enabled self-adaptive hydrogel interface for active electroencephalogram interactions. *ACS Nano* 2022; **16**: 19373–19384.

14 Wang C, Wang H, Wang B, *et al.* On-skin paintable biogel for long-term high-fidelity electroencephalogram recording. *Sci Adv* 2022; **8**: eabo1396.

15 Ren Z, Hu W, Liu C, *et al.* Phase-changing bistable electroactive polymer exhibiting sharp rigid-to-rubbery transition. *Macromolecules* 2016; **49**: 134–140.

16 Guo W, Zheng P, Huang X, *et al.* Matrix-independent highly conductive composites for electrodes and interconnects in stretchable electronics. *ACS Appl Mater Interfaces* 2019; **11**: 8567–8575.

17 Zhao J, Feng J, Jiang Y, *et al.* Skin-integrated electrodes based on room-temperature curable, highly conductive silver/polydimethylsiloxane composites. *Small* 2024; **20**: 2309470.

18 Sun S, Li M, Liu A. A review on mechanical properties of pressure sensitive adhesives. *Int J Adh Adhes* 2013; **41**: 98–106.

19 Chang EP. Viscoelastic properties of pressure-sensitive adhesives. *J Adh* 1997; **60**: 233–248.

20 Wu H, Yang G, Zhu K, *et al.* Materials, devices, and systems of on-skin electrodes for electrophysiological monitoring and human-machine interfaces. *Adv Sci* 2021; **8**: 2001938.

21 Arumugam V, Naresh MD, Sanjeevi R. Effect of strain rate on the fracture behaviour of skin. *J Biosci* 1994; **19**: 307–313.

22 Jiang Y, Wang Z, Kim I, *et al.* Flexible finger-shaped active dry EEG electrode with a configurable application-specific integrated circuit and embedded leadoff detection. *IEEE Sens J* 2023; **23**: 17439–17450.

23 Biasiucci A, Franceschiello B, Murray MM. Electroencephalography. *Curr Biol* 2019; **29**: R80–R85.

24 Gao KP, Yang HJ, Wang XL, *et al.* Soft pin-shaped dry electrode with bristles for EEG signal measurements. *Sens Actuat A-Phys* 2018; **283**: 348–361.

25 Friman O, Volosyak I, Graser A. Multiple channel detection of steady-state visual evoked potentials for brain-computer interfaces. *IEEE Trans Biomed Eng* 2007; **54**: 742–750.

26 Liu J, Liu X, He E, *et al.* A novel dry-contact electrode for measuring electroencephalography signals. *Sens Actuat A-Phys* 2019; **294**: 73–80.